



Published in final edited form as:

Methods Mol Biol. 2016 ; 1445: 77–108. doi:10.1007/978-1-4939-3718-9_6.

Quantitative intracellular localization of cationic lipid-nucleic acid nanoparticles with fluorescence microscopy

Ramsey N. Majzoub, Kai K. Ewert, and Cyrus R. Safinya*

Physics Department, Materials Department and Molecular, Cellular and Developmental Biology Department, University of California at Santa Barbara, Santa Barbara, CA 93117

Summary

Current activity in developing synthetic carriers of nucleic acids (NA) and small molecule drugs for therapeutic applications is unprecedented. One promising class of synthetic vectors for the delivery of therapeutic NA is PEGylated cationic lipid (CL)-NA nanoparticles (NPs). Chemically-modified PEG-lipids can be used to surface-functionalize lipid-NA nanoparticles, allowing researchers to design active nanoparticles that can overcome the various intracellular and extracellular barriers to efficient delivery. Optimization of these functionalized vectors requires a comprehensive understanding of their intracellular pathways. In this chapter we present 2 distinct methods for investigating the intracellular activity of PEGylated CL-NA NPs using quantitative analysis of fluorescence microscopy.

The first method, spatial localization, will describe how to prepare fluorescently-labeled CL-NA NPs, perform fluorescence microscopy and properly analyze the data to measure the intracellular distribution of nanoparticles and fluorescent signal. We provide software which allows data from multiple cells to be averaged together and yield statistically significant results. The second method, fluorescence colocalization, will describe how to label endocytic organelle via Rab-GFPs and generate micrographs for software-assisted NP-endocytic marker colocalization measurements. These tools will allow researchers to study the endosomal trafficking of CL-NA NPs which can guide their design and improve their efficiency.

Keywords

Nucleic acid carriers; PEGylated nanoparticles; Rab GTPase; Particle tracking; Image analysis; Endosomal escape; Transfection; Liposomes; Liquid crystals

1. Introduction

1.1. Background

Lipids are a class of amphiphilic molecules that self-assemble into liquid crystalline phases in aqueous environments at high concentrations (1). The structures of lipid phases are determined by the physical and chemical properties of the individual lipid molecules (2).

*Address for correspondence: Cyrus R. Safinya, Physics Department, Materials Department and Molecular, Cellular and Developmental Biology Department, University of California at Santa Barbara, Santa Barbara, CA 93117, Tel: +1 (805) 893-8635, Fax: +1 (805)-893-7221, safinya@mrl.ucsb.edu.

Energetically favorable assemblies of lipids with distinct shapes are those that minimize exposure of the hydrophobic tails to water due to the hydrophobic effect. Numerous intracellular organelles, along with the cell itself, are enclosed within lipid membranes. These biological membranes are two-dimensional (2D) bilayer structures that are impermeable to water and house membrane-bound proteins which play a variety of essential roles in cellular function (3). Their inherent impermeability allows cellular membranes to act as a barrier so that organelles maintain chemically distinct environments. Shortly after their initial discovery as the major component in plasma membranes (4), biomedical researchers used lipid vesicles, or liposomes, as drug carriers by loading the hydrophobic regions and aqueous interiors with hydrophobic and hydrophilic drugs respectively (5–7). This marked the beginning of lipids as carriers of therapeutic drugs in delivery applications. Although *in vitro* results were promising (8,9), *in vivo* studies showed that the phagocytic system and filtering activity of the liver and kidneys made circulation times brief and impractical (10,11). One approach to prolonging the circulation time of lipid-based drug or nucleic acid (NA) carriers is through surface modification with hydrophilic polymers (12,13). Polyethylene glycol (PEG) satisfies a number of beneficial criteria for use as a surface modification agent in nano-therapeutics; it is charge neutral, hydrophilic and biologically inert (14). When PEG is grafted to surfaces it inhibits adhesion of macromolecules by inducing a repulsive interaction between the surface and macromolecules (15–17). By the same mechanism, PEG-modification of particles in solution prevents aggregation induced by van der Waals-forces, imparting colloidal stability to the modified particle (18). These attributes make PEG-modification (a process often called PEGylation) a promising strategy for developing lipid vectors for delivery applications *in vivo*. Fig. 1 shows the evolution of lipid-based carriers that has occurred in recent decades (19). Initially, liposomes lacking surface modification were used as vectors for hydrophobic and hydrophilic drugs (Fig. 1A). These carriers were replaced by surface-modified liposomes containing polymer-lipids (Fig. 1B). The polymer chains, which extend beyond the surface in a brush conformation, provide a platform for covalent attachment of targeting ligands, allowing liposomes to target specific cell types and facilitate receptor-mediated endocytosis (20,21). Finally, as shown in Fig. 1C, condensed lipid-DNA particles containing both targeting moieties and chemically responsive polymers capable of undergoing cleavage in the low pH environments of late endosomes are being developed as future therapeutics. Lipid vectors using such chemically-modified PEG-lipids are promising candidates for targeted and effective delivery of NA to specific cell types.

1.2. Effects of PEGylation on the structure and assembly of cationic lipids (CL)-DNA complexes

Cationic liposomes and NA spontaneously self-assemble into ordered structures which have been extensively characterized via small angle x-ray scattering (22–28). The CL-DNA complexes' structures are predicted by the curvature elastic theory of membranes (29). The shape of the lipid, which determines the preferred phase of the lipid self-assembly (i.e. L_{α} , H_I , H_{II}) (30–32), can also determine the phase of the CL–DNA complex. In many lipid systems the “shape” of the molecule determines the spontaneous curvature of the membrane ($C_o = 1/R_o$) and also determines the actual curvature $C = 1/R$. The actual curvature describes the structure of the lipid self-assembly where $C = 0$ corresponds to lamellar (L_{α}), $C < 0$

corresponds to inverted hexagonal (H_{II}) and $C > 0$ corresponds to hexagonal (H_I). This model successfully predicts the phase behavior of systems where the rigidity of the membrane is large ($\kappa/k_B T \gg 1$) such that significant deviations of C from C_o would cost elastic energy $(\kappa/2) \cdot (1/R - 1/R_o)^2$ (29). If the bending cost is low ($\kappa \approx k_B T$), then C can deviate from C_o without a large elastic energy cost. This behavior is further driven by the lowering of other energies in the process (e.g. the electrostatic energy between DNA and CL). In the case of DOTAP/DOPC/DNA complexes, the membrane rigidity $\kappa/k_B T$ is of order 10 resulting in the complex assembling into the lamellar L_α^C phase (DOTAP/DOPC membranes have a zero spontaneous curvature (22)). However, the addition of a cosurfactant such as pentanol (molar ratio of about 4:1 cosurfactant to lipid (33)) lowers the bending rigidity ($\kappa \approx k_B T$) so that the system will prefer the inverse hexagonal H_{II}^C phase (23). This occurs because the electrostatic energy gain in transitioning from the L_α^C to H_{II}^C is greater than the energy loss due to C deviating from C_o .

Fig. 2 shows 3 structures that have been reported for different combinations of cationic and neutral lipids with DNA. The lamellar phase shown in Fig. 2A (as well as in Fig. 1C) contains DNA sandwiched between lipid bilayers (22). Fig. 2B shows the H_{II}^C phase where hexagonally-packed inverted cylindrical micelles contain DNA in their aqueous interior (23). Fig. 2C shows the H_I^C phase where hexagonally-packed, cylindrical micelles form a dual lattice with DNA packed in a honeycomb pattern (26). In the case of lamellar complexes, the compositional parameters ρ_{chg} (charge ratio of CL to anionic basepairs (bp)) and σ_m (the membrane charge density, a function of the ratio of cationic to neutral lipid) determine the DNA spacing by modulating the available bilayer area (24).

CLs can also complex and deliver small interfering RNA (siRNA), which is used in post-transcriptional gene silencing (34). Along with the lamellar and hexagonal phases shown in Fig. 2A, B, synchrotron X-ray scattering has shown that CLs and glycerol mono-oleate (GMO) can form cubic phases when mixed with siRNA (35,36). Fig. 3A shows the unit cell of the double gyroid cubic phase where siRNA is contained in distinct water channels (green and orange) that are separated by a lipid surface (grey). The silencing efficiency of vectors in the cubic phase is shown in Fig. 3B where optimal silencing corresponds to K_T (total gene knockdown including sequence specific and non-specific) equals 1 and K_{NS} (non-specific knockdown) equals 0. From Fig. 3B we observe that the cubic phase with $0.6 < K_T < 0.7$ and $K_{NS} < 0.1$ (black squares where the GMO mol fraction Φ_{GMO} is greater than 0.75) significantly outperforms lamellar complexes which are formed with DOPC (black circles). The observed high silencing efficiency of cubic phase complexes at low membrane charge density make it unique in regards to lamellar phase CL–DNA complexes, which only show high efficiency at a high membrane charge density. The non-specific silencing (K_{NS}), a measure of toxicity, is low for both phases (red curves). The proposed mechanism for the high silencing efficiency of cubic phases is that the negative Gaussian curvature of the cubic phase can promote fusion of the complex with the endosomal membrane and subsequent pore formation, resulting in delivery of siRNA molecules to the cytoplasm.

When liposomes are pre-grafted with PEG-lipids and subsequently combined with DNA, the resulting CL–DNA complexes contain PEG-lipid on their interior and exterior. The interior PEG moieties can reduce the DNA-DNA spacing by inducing a depletion attraction force (25). This effect was found to be most pronounced at low membrane charge densities where the DNA-DNA spacing in the absence of PEG-lipid is large and can be reduced by a factor of 2 when 10 mol% of PEG-lipid is incorporated. PEG-lipids not only alter the DNA spacing but can also influence the size of the complexes as well as the total number of layers (25,28,37). In 150 mM NaCl solution, the electrostatic repulsion of like-charged CL–DNA complexes is screened, resulting in fusion of smaller complexes into large aggregates (see Fig. 4A). Incorporating PEG-lipids into these complexes provides a repulsive steric force that prevents fusion and promotes the assembly of stable, sub-100 nm CL–DNA nanoparticles (NPs, see Fig. 4B) that can maintain their size for at least 24 h post-complexation (37). Steric stabilization of CL–DNA particles is essential for developing lipid-based NPs for *in vivo* applications, where NPs are exposed to high ionic strength plasma and subject to filtration by organs upon reaching a critical size.

The polymer-induced steric repulsion also modulates the average number of layers or lamellae in each NP (28). Using small angle x-ray scattering, Silva et al. showed that NP formation is pathway-dependent: the ionic strength of the formation buffer can alter the average number of layers per NP (28). PEGylated liposomes and DNA complexed in the presence of physiological salt concentrations result in NPs containing 5 or fewer layers while complexation in pure water, in the absence of added salt (dH₂O), followed by transfer of NPs into solutions near physiological salt concentrations results in a bimodal distribution of NPs containing either 20–30 or 2–3 layers. The phase diagram provided in (28) shows that by tuning the membrane charge density, PEG grafting density, charge ratio and buffer ionic strength, it is possible to form NPs with a desired number of layers between 2 and 30. While all *in vitro* and *in vivo* applications of PEGylated CL–DNA NPs require they be transferred to physiological buffer, the study by Silva et al. demonstrated that forming NPs in water and transferring them to salt solution enables the preparation of kinetically trapped particles which are unable to reach their equilibrium configuration of only a sparse number of layers at the higher salt concentrations.

A recent cryo-EM study has found that the DNA length and topology can also influence the average number of layers found in each particle (38). NPs formed with long, linear DNA (48 kbps, lambda DNA) or circular plasmid (2 kbps, pDNA) results in more layers than NPs formed with polydisperse, linear DNA (2 kbps, salmon DNA). Furthermore, NPs formed with lambda DNA at low charge ratios (i.e., with excess DNA) in the presence of dH₂O results in DNA-induced tethering of NPs into polymer-mediated flocs.

1.3. Effects of structure and PEGylation of CL–DNA complexes on Transfection Efficiency (TE)

The significance of the discovery of the structure of CL-DNA complexes was highlighted by the finding that the structure of CL-DNA complexes affects their function (39). Confocal imaging and TE assays showed that while H_{II}^C (inverse hexagonal) complexes are capable of undergoing direct fusion with the plasma membrane, lamellar complexes are taken up by

cells through endocytosis (39). Upon endocytosis, complexes are trafficked via endosomes and their efficacy is limited due to their degradation in lysosomes barring their escape from endosomes into the cytoplasm (37,40). Endosomal escape, the bottleneck to efficient therapeutic delivery, occurs through fusion of the endosomal membrane and outer cationic bilayer of the complex. Complexes with high membrane charge density (σ_m = total charge per membrane area, a parameter that depends on the ratio of cationic to neutral lipids as well as lipid valency and headgroup area) escape endosomes more efficiently and exhibit higher TE (40). Fig. 5A shows the TE of various CL–DNA complexes plotted against their membrane charge density. The data is divided into 3 regimes: at low membrane charge density (Regime 1), complexes mostly remain trapped in endosomes; at moderate membrane charge density (Regime 2), complexes escape endosomes and undergo disassociation (release of DNA from the complex) and finally, at high membrane charge densities (Regime 3), complexes escape endosomes but fail to undergo complete disassociation due to a strong electrostatic interaction between CLs and DNA. As mentioned above, the TE of H_{II}^C complexes (hollow symbols in Fig. 5A) does not depend on their membrane charge density, implying that endosomal escape is not a bottleneck to efficient transfection for these complexes. The dependence of TE on structure and membrane charge density (in the case of lamellar complexes) provides guidelines for the optimal formulation of effective CL–DNA complexes.

For *in vivo* applications of CL–DNA complexes, PEGylation is required to extend circulation times. However, the addition of PEG-lipids significantly alters the interactions of CL–DNA complexes with cellular membranes such as the plasma membrane and the compositionally-related endosomal membrane (37). Fig. 5B shows the TE of CL–DNA NPs with moderate membrane charge density as a function of mol% PEG2K-lipid. As PEG-lipid increases beyond 5 mol% (coinciding with the grafting density that marks the transition of the PEG chains from the mushroom to the brush conformation), a significant drop in TE occurs. Two plausible explanations for this drop in TE are (1) the PEG corona around individual NPs obstructs adhesion of NPs to the plasma membrane, reducing cell uptake and (2) PEG-induced steric repulsion between the NP and endosomal membrane inhibits fusion between the two.

Custom-synthesized PEG-lipids allow the formulation of NPs designed to overcome these barriers to efficient transfection. Cellular attachment may be recovered by grafting a ligand or peptide sequence to the distal of the PEG moiety, allowing NPs to bind to receptors on the plasma membrane (37). One class of targeting peptides that has shown significant success both *in vitro* and *in vivo* is based on the arginine-glycine-aspartic acid (RGD) motif (41). RGD peptides have a specific interaction with integrin receptors which are frequently over-expressed in cancer cells, making them an ideal candidate for peptide-mediated targeting of tumors (42,43). As shown in Fig. 5C, RGD-tagging of CL–DNA NPs partially recovers the TE that is lost when CL–DNA complexes are PEGylated. PEG-lipids with a pH-sensitive linker that is capable of undergoing hydrolysis (named HPEG: hydrolyzable PEG-lipid) in the late endosomal environment allows NPs to shed their PEG corona, fuse with the endosomal membrane and access the cytoplasm for efficient release of cargo (44). Fig. 5D

shows the TE of HPEGylated CL–DNA NPs as a function of ρ_{chg} . As observed for RGD-tagged NPs, TE partially recovers.

The similarity of the TE results for RGD-tagged NPs and HPEGylated NPs despite their differing chemistry and design concepts highlights the need for a more informative experimental technique for studying NP uptake and intracellular processing. While the TE assay is a high-throughput and sensitive technique for measuring the efficacy of gene transfer and subsequent expression, robust optimization of vectors requires the ability to discriminate between the major bottlenecks to transfection.

1.4. Quantitative imaging of fluorescently-labeled CL–DNA NPs

Fluorescence microscopy has been instrumental in understanding biological processes. Specific labeling of biological components through fluorescent tagging allows direct observation of biological interactions *in situ*. Fluorescence microscopy of cells incubated with CL–DNA NPs allows investigations of pathways and barriers, thus enabling better chemical design and formulation. One common strategy when performing fluorescence microscopy with NA vectors is dual labeling, where a fluorescent lipid is used to label and track lipids while a separate dye (with distinct excitation and emission) is covalently attached to the NA for tracking the fate of the NA cargo. Dual fluorescent labeling permits discrimination between CL–DNA NPs and cationic liposomes lacking DNA (which coexist at equilibrium, *see* Fig. 4B) (24,38). Furthermore, dual-labeled CL–DNA complexes allow direct visualization of vector-cargo disassociation (39,45).

The value of qualitative imaging for yielding mechanistic insights is limited in systems as complex as cells undergoing transfection. Rather, a comprehensive understanding of intracellular NP behavior requires extracting quantitative data from fluorescence micrographs. One issue in obtaining statistically meaningful results through quantitative imaging of cells is the inherent cell-to-cell variability which produces random error. Thus it is necessary to use computer software to automate the measurements and allow data to be extracted from large numbers of cells. As of today, numerous research groups use quantitative analysis of fluorescent imaging to study gene delivery vectors (37,38,44,46–51). Intracellular localization is an interesting feature that can be measured from fluorescence microscopy. Localization allows the spatial distribution of NPs to be measured, so that the accumulation of NPs in the perinuclear region (a frequent characteristic of NPs with poor early endosomal escape) can be quantified. We have developed image analysis routines in Matlab for performing this quantification (37,38,44). Fig. 6A,B provides an example of the software's functionality. First, the user defines the boundary of a cell in the fluorescent image using the plasma membrane-bound NPs that form an outline of the cell in the current focal plane (Fig. 6A). Alternatively, the cell boundary can be determined via a brightfield image. Second, the nuclear membrane is identified by the user in the bright field image so that it may be used as a reference point, allowing data from multiple cells to be averaged (Fig. 6B). Next, the routine automatically detects and localizes fluorescent NPs using algorithms from (52). Finally, the software defines regions of the cell which are equidistant to the nuclear membrane and counts the number of NPs in each region (37). The routine is also capable of measuring the total number of NPs per cell by integrating over the

localization curves at each time point (37). This feature is useful when NPs cannot be effectively washed off the outside of the cell, where methods such as flow cytometry would measure the total fluorescence intensity of cell-associated NPs as opposed to cell-internalized NPs. Although our software can also measure internalization by measuring net fluorescence, object-based colocalization (where individual NPs are counted) is preferable because it produces consistent results independent of fluorescent label density, camera settings or photobleaching.

Fig. 6C presents intracellular localization data which shows the average number of particles found at a given distance to the nuclear membrane for PEGylated NPs, RGD-tagged NPs and HPEGylated NPs. The results show that RGD-tagged NPs are taken up by cells more efficiently than PEGylated and HPEGylated NPs. When comparing HPEGylated NPs to PEGylated NPs, we see similar uptake at early time points ($t = 2$ h). However, as individual NPs escape the endosome (in the case of HPEGylated NPs), more NPs are spatially resolvable and counted. Fig. 6D–I contains examples of the DIC and fluorescent micrograph used to generate the data shown in Fig. 6C. The TE of RGD-tagged and HPEGylated NPs are similar, but quantitative imaging shows significant differences (37,44). This implies that HPEGylation and RGD-tagging improve TE through distinct mechanisms. RGD NPs are internalized more efficiently than HPEGylated NPs. Thus, the image analysis suggests that RGD-tagging of NPs partially recovers TE relative to PEGylated NPs due to high uptake (37), while HPEGylated NPs partially recover TE due to efficient endosomal escape (44). We see perinuclear accumulation in all 3 cases, indicating that the NPs are inside endosomes which are being trafficked by motor proteins. In the case of HPEGylated NPs, they are trafficked by early endosomes to the perinuclear region before the endosome matures and lowers its pH, allowing NPs to shed their PEG coat and escape endosomes. Quantitative fluorescent imaging thus allows discrimination between NP formulations which show low TE due to inefficient uptake or endosomal escape.

Another powerful application of quantitative image analysis is the study of colocalization, in particular for deciphering endocytic pathways. Escape from endosomes is a limiting step in transfection with CL–DNA complexes and is strongly affected by PEGylation (37,44). Thus, it is highly desirable to have a means for investigating the endosomal trafficking and escape properties of lipid-based NPs. Fluorescence imaging can be used to quantify colocalization of NPs and fluorescently-tagged organelles, allowing unambiguous determination of the NP's intracellular pathway as well as measurement of intracellular targeting efficiency. One promising approach is direct labeling of various endocytic stages using the Rab family of enzymes (53–55). Rab GTPases mediate budding, trafficking and fusion of membrane-bound organelles, with over 70 distinct Rab proteins in humans reported to date (56). Each Rab GTPase associates with a distinct stage of the endosomal pathway, allowing discrimination between NPs found in early, recycling or late endosomes.

Fig. 7 features fluorescence micrographs and cropped regions of wildtype Rab5-GFP (*see* Fig. 7A, C) and mutant Rab5-GFP-Q79L (*see* Fig. 7B, F) expressing mouse L-cells that have been incubated with dual-labeled NPs. In the case of wildtype Rab5, early endosomes appear as small, diffraction-limited spots in the green channel (*see* Fig. 7A). The cropped region (*see* Fig. 7C) and corresponding intensity scan (*see* Fig. 7D) show 2 classes of

fluorescent signal. The first signal (Fig. 7C, D (i)) is from a NP that lacks Rab5-GFP colocalization, while the other 2 objects (Fig. 7C, D (ii, iii)) are NPs colocalized with GFP-Rab5, implying that they are inside early endosomes (53). We have developed a software routine that counts the fraction of total intracellular NPs inside fluorescently labeled endosomes. Our analysis uses an object-based colocalization algorithm that measures the number of NPs that are inside versus outside of GFP-labeled endosomes based on the distance between a NP and the closest endosome. Pixel-based colocalization methods (Pearson's coefficient, Mander's coefficient (57)) are useful measures for comparing colocalization of fluorescent proteins but our method provides nanoparticle statistics, which allows direct mapping of an NP's intracellular pathway. Much like the localization algorithm described above, object-based colocalization is insensitive to photobleaching, camera settings and variations in fluorescent label per NP. Fig. 7E shows an example of the resulting data for the early endosome marker, Rab5, at an early time point (60 min). In the case of wildtype Rab5, only a small fraction of NPs are found to be colocalized with early endosomes.

Fig. 7 B, F show a micrograph and cropped region of a cell expressing mutant Rab5-Q79L-GFP. In contrast to wildtype Rab5, cells expressing the mutant Rab5-Q79L show nearly all intracellular NPs are within early endosomes or giant early endosomes (GEEs). The Q79L mutation of Rab5 inhibits GTP hydrolysis, increasing the early endosome's size and lifetime. The results with the mutant Rab5 show that the lack of colocalization of NPs with wildtype Rab5-GFP is due to the short lifetime of early endosomes and not indicative of escape from early endosomes; if NPs could escape early endosomes, we would expect to see more NPs outside of the GEEs that are present when the mutant Rab5-Q79L is used. The slow maturation and spatially resolvable size of the GEEs that form with the mutant Rab5 make it a powerful assay for measuring NP escape from early endosomes. Wildtype Rab5 is not an ideal marker for measuring escape from early endosomes because intracellular NPs that lack Rab5 colocalization could be in a later endosomal compartment (e.g., late or recycling endosomes).

Below we provide protocols for preparing fluorescent CL-DNA NPs and imaging the transfection of mammalian cells *in vitro* using optical microscopy. We also describe how to perform the analysis shown in Fig. 6 and 7 using our custom-developed software routines. All the routines were developed in Matlab and are provided as m-files at <http://www.mrl.ucsb.edu/~safinyaweb/lab.htm>. We encourage users to modify and implement the routines to their liking.

2. Materials

2.1. Liposome Preparation

1. 9:1 (v:v) Chloroform:methanol (CHCl_3 :MeOH) mixture.
2. 15:13:2 (v:v:v) CHCl_3 :MeOH:dH₂O mixture.
3. High-resistivity water.

4. Desired lipids to be used (e.g., DOTAP, MVL5, DOPC, PEG2K-DPSE) as solids (*see* Note 1).
5. Fluorescently-tagged lipid (*see* Note 2).
6. 1.5 mL vials with Teflon-lined caps (*see* Note 3).
7. Oven at 37°C.
8. Nitrogen (N₂) stream.
9. Rotary evaporator.
10. Tip sonicator.

2.2. Imaging Assays

1. Liposome solutions.
2. 100 µg/mL stock solution of NA (*see* Note 4).
3. Solution of fluorescently labeled NA (*see* Note 5).
4. Appropriate formation buffer for CL–DNA complexes (cell culture medium or water at desired salt concentration).
5. 1.5 mL polystyrene microcentrifuge tubes.
6. Tweezers.
7. 22 × 22 mm No. 1.5 coverslips and 6-well plates or glass bottom dishes (GBDs) (*see* Note 6).
8. Poly-(L-lysine) solution (molecular weight (MW): 30,000–70,000 g/mol, 0.1% (wt/v) solution).
9. 7× cleaning solution
10. Ethanol (EtOH), 190 proof (100% EtOH).
11. 70/30 (v/v) EtOH/dH₂O mixture (70% EtOH).
12. Sterile plastic petri-dishes.
13. Phosphate buffered saline (PBS).
14. Serum-free cell culture media (e.g., DMEM, RPMI).

¹Avanti Polar Lipids sells lipids in powder form or as CHCl₃ solutions. If starting with lipids already dissolved in CHCl₃, then dilute to the appropriate concentration.

²We typically use TRITC-DHPE or Texas Red-DHPE from Life Technologies. These dyes do not have spectral overlap with GFP or Cy5, which are used to label endosomes and DNA, respectively.

³Teflon lining minimizes solvent evaporation. We recommend vials with conical bottoms to maximize the volume that can be recovered from the vials.

⁴We have had success purchasing our pDNAs from addgene.org and propagating in *Escherichia Coli* (*E. coli*) using the kits and protocol provided by Qiagen. Purification from *E. coli* is done using a Mega or Giga Kit from Qiagen. pDNAs in aqueous solution can be stored in the freezer for years. A suitable stock concentration is 250 µg/mL.

⁵Labeling DNA is done using the Mirus Label IT Nucleic Acid Labeling Kit. We follow the manufacturer's protocol with the only modification being an extension of the 37°C incubation to 2 h, thereby increasing the labeling efficiency.

⁶Coverslips are eventually mounted to microscope slides and used for fixed cell imaging. Glass-bottom dishes (MatTek) are used for live cell imaging.

15. Cell culture media supplemented with fetal bovine serum (complete medium).
16. Enzyme-free disassociation buffer (Therrno Fisher Scientific, Waltham, Massachusetts).
17. Hemocytometer.
18. Lipofectamine 2000 (L-2000) or alternative transfection reagent.
19. Rab-GFP pDNA (*see* Note 7).
20. Solution of “non-coding” DNA (e.g., calf thymus or salmon sperm DNA).
21. Refrigerator at 4°C.
22. 50 U/mL Heparin sulfate in PBS (*see* Note 8).
23. Microscope equipped for fluorescent imaging.
24. Mounting medium.
25. Mammalian cells (e.g., HeLa, PPC-1, M-21, etc.)

2.3. Software

1. ImageJ (with PSF Generator and Iterative Deconvolve 3D plug-ins).
2. Matlab (with Image Processing Toolbox).

3. Methods

3.1. Liposome Preparation

Relevant Parameters (parameters marked with * are set by the user and can be varied):

Z_{CL} : Charge of the CL (e.g. MVL5: $Z_{CL}=5$, DOTAP: $Z_{CL}=1$).

MW_{CL} : MW of the CL.

MW_{NL} : MW of the neutral lipid.

MW_{FL} : MW of functional lipid (e.g PEG2K-lipid, RGD-PEG2K-lipid).

Φ_{CL} : Mol fraction of CL (determines membrane charge density)*.

Φ_{FL} : Mol fraction of functionalized PEG-lipid (determines PEG coverage and conformation)*.

Φ_{NL} : Mol fraction of neutral lipid ($=1 - \Phi_{FL} - \Phi_{CL}$).

C_S : Concentration of lipid stock solution (in mM/L)* (This can be optimized depending on m_{NA} , ρ , V_F and number of experiments to be performed (*see* Note 9)).

⁷Over 70 types of Rab proteins have been identified in humans, we suggest starting with Rab 5 or Rab 7 which label early and late endosomes, respectively.

⁸Heparin sulfate solution removes most extracellular NPs. Purchase Heparin Sulfate as a powder (Sigma-Aldrich) and form stock solutions at 2,000 U/mL in dH₂O. Prepare a working solution of 50 U/mL in PBS the day of the experiment.

V_S : Volume of lipid stock solution (in μL)* (*see* Note 10).

c_{NA} : Concentration of stock NA (in $\mu\text{g}/\text{mL}$).

ρ_{chg} : Desired CL/NA charge ratio (ratio of positive charges (from CL) to negative charges (from NA))* (*see* Note 11).

m_{NA} : Desired mass of NA to be complexed (in μg) (*see* Note 12).

V_{TL} : The total volume of lipid suspension used to form CL–DNA NPs.

V_{F} : Total volume of buffer containing CL–DNA complexes* (*see* Note 13).

m_{L} : Total mass of lipid to be delivered (determined by m_{NA} and ρ).

Based on the chosen Φ_{CL} , Φ_{NL} , Φ_{FL} , V_S , and C_S , the user will form a stock solution of liposomes. Using the liposome stock solution, the user can prepare multiple samples of CL–NA complexes, where the desired m_{NA} and ρ will determine the volume of liposome stock solution required per sample.

3.1.1. Forming stock solutions of lipids in organic solvents

1. Based on individual lipid stock solution volume (V_{CL}) and concentration (M_{CL}), determine how much lipid to weigh: e.g., $m_{\text{CL}} = M_{\text{CL}} \times V_{\text{CL}} \times MW_{\text{CL}}$ (*see* Note 14).
2. Weigh out the lipid into a glass vial (*see* Note 15).
3. Dissolve the lipid in the appropriate volume of organic solvent (e.g., V_{CL}) (*see* Note 16 and 17).
4. Repeat steps 1–3 for all lipids to be used in the formulation.

⁹Before choosing a liposome concentration we suggest calculating formulations from **Subheading 3.1** (*see* Note 25) to ensure that the liposome solution is at reasonable concentration for making complexes. For liposomes containing monovalent lipids at 50 mol%, a concentration of liposomes at 2 mM allows formation of NPs with reasonable volumes. Fluorescently-labeled liposomes are used in much smaller quantities such that the stock solution of liposomes could be prepared at 500 μM .

¹⁰If using a tip sonicator to generate small vesicles, there is typically a lower limit on V_S such that the sonicating tip can be sufficiently submerged. Otherwise the volume can be optimized depending on m_{NA} , ρ , V_{F} and number of experiments to be performed.

¹¹The molar charge ratio of CLs to anionic DNA sets the effective charge of the CL–DNA NPs. Above the isoelectric point ($\rho_{\text{chg}} \approx 1$), the NPs have a net positive charge. At high charge ratios ($\rho_{\text{chg}} > 1$), the NPs coexist with cationic liposomes at equilibrium.

¹²When forming samples for imaging, each well (or GBD) uses 0.1 μg of labeled DNA and 3 μg of unlabeled DNA (*see Subheading 3.3.3, 3.3.4 or 3.3.5*).

¹³The total volume of complexes depends on the size of the wells that the cells will be seeded in. For 6-well plates, add 2 mL/well of culture medium and then add 500 μL /well of complex solution. For 24-well plates, complexes are formed in 200 μL /well of culture medium and added to empty wells.

¹⁴As an example, if the CL is MVL5 ($MW_{\text{MVL5}} = 1164.86 \text{ g}/\text{M}$) and you want a stock solution at 2 mM M_{CL} with 1 mL of V_{MVL5} , then $m_{\text{MVL5}} = (2 \text{ mM}) \times (1 \text{ mL}) \times (1164.86 \text{ g}/\text{M}) = 2.33 \text{ mg}$. If you do not have a scale with necessary precision to weigh such small amounts, a more concentrated stock solution can be made and diluted to yield the appropriate CL stock solution concentration.

¹⁵Some lipids are hydroscopic and will stick to the spatula. We recommend using 2 spatulas; one to scoop lipid from container while the other is used to scrape lipid off the first spatula into the new vial.

¹⁶Most cationic and neutral lipids readily dissolve in 9:1 (v/v) CHCl_3 :MeOH. We have found that peptide-PEG-lipids dissolve more readily in mixtures of CHCl_3 , MeOH and dH_2O , e.g., 65:23:2 (v/v/v) CHCl_3 :MeOH: dH_2O .

¹⁷We suggest filling and emptying the pipette tip once or twice before aspirating the desired volume. This prevents dripping of the organic solvent from the pipette tip due to its low vapor pressure.

3.1.2. Liposome formation

1. Calculate the required volume lipid stock solutions (*see Subheading 3.1.1*) to combine:

$$V_{CL} = V_S \times (C_S / M_{CL}) \times \Phi_{CL}$$

2. Calculate the additional volume of solvent (V_{sol}) needed to achieve V_S , according to the following formula:

$$V_{sol} = V_S - (V_{CL} + V_{NL} + V_{FL})$$

3. Add V_{sol} of organic solvent to a new glass vial. Then pipette the calculated volumes of lipid stock solutions into the vial (*see Note 17 and 18*).
4. Calculate the total weight of cationic and neutral lipids in V_S and add 0.2 wt% of fluorescent lipid to V_S (e.g., $m_{FL} = V_S \times C_S \times (\Phi_{CL} \times MW_{CL} + \Phi_{CNL} \times MW_{NL})$) (*see Note 19 and 20*).
5. Use a N_2 stream (or rotary evaporator for large volumes) to evaporate the 9:1 (v:v) Chloroform:methanol mixture and form a lipid film on the side of the vial (*see Note 21*).
6. To ensure complete removal of organic solvent, place the vial containing the dried lipid film in a vacuum desiccator for at least 8 h.
7. Add V_S of dH_2O or desired buffer to the vial containing the lipid film.
8. To ensure complete hydration of the lipid film, close the vial tightly, seal the lid with parafilm, and incubate overnight in an oven at $37^\circ C$ (*see Note 22*).
9. Remove lipid solutions from the incubator and sonicate with a tip sonicator (*see Note 23 and 24*).
10. After tip sonication, filter liposome solution (*see Note 25 and 26*). Store at $4^\circ C$ until use.

¹⁸When adding lipid solutions, pipette up and down so that the solvent added as V_{sol} can rinse off any lipid solution that adhered to the inside of the pipette tip.

¹⁹When the stock solutions of fluorescent lipid are at 1 mg/mL, a typical volume of fluorescent lipid on the order of 1 μL is added to a V_S of 500 μL at 1 mM.

²⁰The weight fraction of fluorescent lipid has to be adjusted based on the sensitivity of the imaging system. We recommend using the least amount of fluorescent lipid that makes imaging feasible.

²¹If drying via nitrogen stream use the fastest speed that does not splash solution out of the vial. Slow speeds result in thick films which are hard to dry and hydrate.

²²If using lipids that have a higher transition temperature, incubate in an oven at a temperature such that all lipids are in the liquid phase.

²³After incubation, the lipid solutions may appear cloudy or turbid due to the formation of large multilamellar vesicles (LMVs). Sonication promotes the formation of SUVs.

²⁴We strongly recommend a tip sonicator instead of an ultrasound bath sonicator, which in our experience is not powerful enough.

²⁵A 200 nm filter will remove metal debris deposited by the tip sonicator.

²⁶After a period of 2–4 wks it is strongly suggested to resonicate the liposome suspension to ensure that the liposomes remain as small unilamellar vesicles (SUVs).

3.2. Rab-GFP Expression in Mammalian Cells

3.2.1. Preparation of coverslips or glass bottom dishes—Glass bottom dishes are packaged as sterile and do not require the cleaning steps outlined below in steps 1–10.

1. Using clean tweezers, pick individual coverslips from their casing and drop them into a beaker containing a solution of soap (we recommend 7× cleaning solution) and dH₂O.
2. Sonicate in a bath sonicator for 15 min.
3. Discard soap-dH₂O mixture and rinse coverslips 3 times with dH₂O. Perform rinsing by discarding dH₂O, replacing with fresh dH₂O and swirling for 5–10 sec.
4. Sonicate the coverslips in dH₂O.
5. Discard the dH₂O and rinse the coverslips 3 times with dH₂O.
6. Add 70% EtOH to the coverslips and sonicate them.
7. Discard 70% EtOH and rinse the coverslips once with 70% EtOH.
8. Add 100% EtOH to the beaker, cover the beaker with aluminum foil, and store it at room temperature (RT).
9. To dry the coverslips, place a clean piece of aluminum foil in an oven at 37°C or 60°C, remove individual coverslips from 100% EtOH, and place them on the aluminum foil for 10–15 min.
10. Using tweezers, remove the dried coverslips from the oven and place them in a plastic petri-dish.
11. Apply 500 μL of poly-(L-lysine) solution to each coverslip (or GBD well). Spread the solution with the pipette tip to ensure full surface coverage of the poly-(L-lysine) solution (*see Note 27*).
12. Gently shake the petri-dish for 15 min.
13. Aspirate excess poly-(L-lysine) solution and rinse coverslips (or GBD wells) by adding dH₂O and gently swirling.
14. Aspirate the dH₂O and repeat the rinsing step with PBS.
15. Aspirate the PBS and perform the rinsing step with dH₂O.
16. Place petri-dish containing coverslips (or GBD wells) in an oven at 37°C or 60°C for 2 h to dry.

²⁷We strongly advise against coating with fibronectin or other proteins which contain RGD sequences when performing studies with RGD-tagged NPs. Variations in fibronectin concentration are hard to control and will affect the reproducibility.

3.2.2. Cell seeding

1. When using coverslips, remove coverslips from petri dish (*see Note 28*). Using tweezers, place single coverslips in the wells of a 6-well plate; ensure that the poly-(L-lysine) coated side is facing up.
2. Add 2 mL of serum free medium to each well containing a coverslip (or each GBD well) and then place 6-well plate (or GBD wells) in the incubator for 20 min.
3. Remove a cell culture flask containing cells at > 80% confluency from the incubator and discard the medium.
4. Wash the cells 3 times with PBS, then aspirate and discard the PBS.
5. Add enzyme-free disassociation buffer (EFDB) to the cell culture flask and incubate for 3–5 min at 37°C (*see Note 29*).
6. Aspirate EFDB and firmly tap the sides of the culture flask to dislodge the cells.
7. Resuspend the cells by thoroughly rinsing the bottom of the flask with complete medium. Visually inspect the flask to ensure all cells are detached and suspended in solution.
8. Measure cell density using a hemocytometer and prepare a stock suspension of cells at the appropriate density, typically between $1.8\text{--}2 \times 10^5$ cells/mL (*see Note 30*).
9. Take the 6-well plate (or GBD wells) from the incubator and discard the medium.
10. Apply 2 mL of cell suspension to each well and gently rock back and forth to ensure an even distribution of cells in each well (*see Note 31*).
11. Place the 6-well plate containing cells (or GBDs) in the incubator.

3.2.3. Cell transfection with Rab pDNAs

1. Add 250 μL of serum-free medium into polystyrene microcentrifuge tubes. Use 2 microcentrifuge tubes for each well that is to be transfected with a Rab pDNA.
2. In one polystyrene microcentrifuge tube, add the appropriate amount of L-2000. We found that 10 μL /well (or GBD) of L-2000 achieves reasonable expression without excessive toxicity (*see Note 32*).

²⁸Drying the coverslips can result in them adhering to the petri-dish. Gentle deformation of the petri-dish will help detach them, but take care not to fracture the coverslips in the process.

²⁹We do not recommend detaching cells with Trypsin. Trypsin acts by cleaving integrins, and although cells do eventually replenish integrins, results are more easily reproducible with enzyme-free disassociation buffer from Life Technologies.

³⁰The number of cells plated per well should be adjusted depending on the cell line's growth rate. The optimal seeding density is one where cells are 80% confluent on d 5.

³¹Avoid swirling the wells, as this causes cells to accumulate in the center. Avoid vigorous agitation, as this causes cells to be seeded underneath the coverslips.

3. To the other microcentrifuge tube, prepare the DNA mixture by adding 2 μg of “non-coding” DNA (e.g., calf thymus or salmon sperm DNA) followed by 2 μg of the pDNA. Gently pipette up and down to ensure homogenous mixing (*see* Note 33).
4. Add the L-2000 containing solution to the DNA mixture, and pipette up and down to promote mixing and complexation.
5. Incubate the L2000-DNA mixture for 20 min at RT.
6. Remove cells from the incubator, aspirate the old medium, rinse with PBS and add 2 mL of fresh serum-free medium.
7. Add the L2000-DNA mixture to the wells (or GBDs) by gently dropping the suspension across various regions of each well (or GBD) and gently agitate to ensure a homogenous distribution of the NPs.
8. Incubate the 6-well plate (or GBDs) for 4–6 h at 37°C.
9. Take the 6-well plate (or GBDs) out from the incubator, discard the old culture medium, rinse with PBS and add fresh complete medium (*see* Note 34).
10. Incubate for additional 18–24 h.

3.3. Optical Fluorescence Microscopy

3.3.1. General protocol to form complexes (*see* Note 35)

1. Using the desired charge ratio (ρ) and mass of NA m_{NA} , calculate the volume of the master liposome stock solution required (*see* Note 36).

³²Other transfection reagents can be used in place of L-2000. We recommend optimizing the transfection settings such that (1) minimal toxicity occurs (2) GFP-expression is not heterogeneous and (3) cells are not over-expressing GFP-Rabs. To rule out over-expression, ensure that cells expressing GFP-Rab show similar uptake and particle localization as control cells that have not been transfected with GFP-Rab.

³³GFP-Rab pDNAs are diluted with “filler” DNA to prevent overexpression without significantly reducing the total number of cells that express GFP-Rab.

³⁴If cells are below 70% confluency, complete medium can be added instead of serum-free medium at this step. We prefer synchronizing our cells through serum starvation to minimize variations in cell volume. We strongly suggest not starting the imaging experiment on d 4. Cells need to recover from L-2000 transfection.

³⁵We describe 3 strategies for labeling NPs and performing fluorescent imaging. Method 1 is recommended for observing initial endocytic events at early time points ($t < 1$ h). Method 2 allows users to track NPs that are in similar stages of the endocytic pathway by synchronizing their uptake into cells. In contrast to the first method, the second method ensures that cells are exposed to the same concentration of NPs as used in transfection experiments. Method 3 completely mimics a transfection experiment in terms of NP concentration but results in a steady stream of NPs being internalized during the 6 h incubation, which can obfuscate results by having individual fluorescent NPs internalize at any time point between 1 and 6 h. Methods 1 and 2 avoid the ambiguity of a distribution of NP-internalization times by cold-incubating the NPs with cells. In the case of PEGylated NPs with and without RGD-tagging, cold incubation allows NPs to settle and coat cells while endocytosis is inhibited. When NPs in solution are removed and cells transferred to a 37°C incubator all cell-associated fluorescent NPs are on the outside of the plasma membrane.

³⁶For a typical imaging experiment we might use $m_{\text{NA}} = 100$ ng of DNA at $\rho = 10$. To calculate the volume of lipid required (V_{TL}):

$$V_{\text{TL}} = m_{\text{NA}} \times (MW_{\text{CL}} \times Z_{\text{BP}} / (MW_{\text{BP}} \times Z_{\text{CL}})) \times \rho \times (100 / \Phi_{\text{CL}}) \times (1 / MW_{\text{CL}}) \times (1 / M_{\text{S}})$$

where Z_{BP} and MW_{BP} the charge and MW of NA base pairs, respectively. $Z_{\text{BP}} = 2$ for DNA and $MW_{\text{BP}} = 660$ g/mol for long double-stranded DNA, but for short DNA (such as oligonucleotides, which are typically ~20 bps long) MW_{BP} must be calculated based on the sequence.

2. Calculate the desired m_{NA} and dilute the corresponding volume of NA stock solution in the desired buffer such that the final volume of DNA solution is 50 μL (*see* Note 37).
3. Dilute the desired amount of lipid solution in the appropriate buffer such that the final volume is 50 μL (*see* Notes 36 – 38).
4. Add 50 μL of the DNA solution to the liposome solution and gently pipette up and down.
5. Incubate the NP solution for 20 min at RT.

3.3.2. Single Pulse of completely labeled NPs

1. Prepare fluorescent NPs by mixing the appropriate amount of fluorescently labeled liposome suspension with fluorescently labeled DNA (*see* Note 5). Add 0.1 $\mu\text{g}/\text{well}$ (or GBD) of labeled DNA, and calculate the lipid amount based on the desired ρ and membrane charge density (*see* Note 36).
2. Take the 6-well plates (or GBDs) out from incubator, discard the old medium, rinse with PBS and add 2 mL/well of cold (4°C) serum-free medium to the cells.
3. Add the NPs to cells by dropping solution across different regions of the well. Gently agitate the dish to ensure the NPs are homogeneously distributed throughout each well.
4. Place cells in a 4°C refrigerator for 1 h (*see* Note 35).
5. Take the 6-well plates (or GBDs) out from the refrigerator and place them in the incubator for the desired time (typically 60 min).

3.3.3. Cell fixation with formaldehyde

1. Remove the 6-well plates (or GBDs) from incubator and discard the old medium.
2. After formaldehyde fixation, wash the cells 3 times with PBS, then incubate them in 2 mL PBS for 3–5 min at RT.
3. Discard the PBS, add the mounting medium and mount the coverslips to microscope slides.
4. Place the samples on the microscope stage and take pictures of them.

3.3.4. Pulse-Chase with labeled and unlabeled NPs

1. Follow the protocol reported in **Subheading 3.2.2.**

³⁷Forming NPs in dH_2O before transferring into cell culture media results in NPs with a larger number of layers than forming the NPs in culture media (*see* **Subheading 1.2** or (28) for more information).

³⁸Liposome suspensions are typically formed under the assumption they will be used for multiple experiments. For example, 10–50 μL out of 500 μL are typically used to form NPs for a single experiment. If lipid material is precious and must be conserved, reduce V_S or C_S . (*see* Note 2).

2. In the meanwhile, prepare unlabeled NPs by mixing the appropriate amount of liposome suspension with unlabeled DNA. Add 3 μg /well (or GBD) of labeled DNA, and calculate the lipid amount based on the desired ρ and membrane charge density (*see* Note 36 and 37).
3. After 60 min of incubation, take the 6-well plates (or GBDs) out from the incubator.
4. Wash the cells twice with ice-cold 50 U/mL heparin solution and once with PBS.
5. Add 2 mL/well of warm (37°C) serum-free DMEM to the cells.
6. Add the unlabeled NPs to the cells and incubate them at 37°C for the desired time (1–6 h).
7. Image live cells or fix cells at the desired time point (*see Subheading 3.3.2*, step 6).

3.3.5. Simultaneous co-administration of labeled and unlabeled NPs

1. Prepare fluorescent NPs by mixing the appropriate amount of fluorescently labeled liposome suspension with fluorescently labeled DNA (*see* Note 5). The final amount of labeled DNA to add to each well is 0.1 μg , and the amount of lipid is calculated based on the desired ρ and membrane charge density (*see* Note 36).
2. Prepare unlabeled NPs by mixing the calculated amount of unlabeled liposome solution with unlabeled DNA. The total amount of unlabeled DNA to add to each well is 3 μg , and the lipid amount is calculated based on the desired ρ and membrane charge density (*see* Note 36 and 39).
3. After incubating labeled and unlabeled NPs for 20 min, take the 6-well plates (or GBDs) out from the incubator, discard the old medium, wash the cells with PBS and add 2 mL/well of warm. serum-free media to them.
4. Mix labeled and unlabeled NPs by repeated pipetting up and down.
5. Add the mixed NPs to the cells and incubate at 37°C for the desired time.
6. Image live or fixed cells (*see Subheading 3.3.2*, step 6).

3.4. Intracellular Localization Analysis

If 3D imaging is performed (using a spinning disk or laser confocal microscope), then image stacks should be processed via a deconvolution algorithm. Below we briefly describe one protocol for doing so, but numerous alternatives are available.

³⁹pGFP can be used as a reporter gene.

3.4.1. Deconvolution and Image Processing

1. Generate PSF: Download and install the ImageJ plugin “Generate PSF”, run the plugin and generate individual PSFs for each fluorescent channel that was imaged (*see Note 40*).
2. Download and install the ImageJ plugin “Iterative Deconvolve 3D”. Run the plugin and select the desired image stack and PSF to be used (*see Note 41*).

3.4.2. NP localization—Localization requires a pair of 2D images for each cell to be analyzed. One should be an 8-bit TIFF file of the bright field image in which the edge of the cell and nuclear membrane are clearly visible. The second image should be an 8-bit TIFF file of the fluorescent image showing NPs as resolution-limited spots. Our website (<http://www.mrl.ucsb.edu/~safinyaweb/lab.htm>) provides links to the 4 m-files necessary for performing localization analysis. The files `pkfnd.m` and `cntrd.m` are Matlab versions of the software developed by Eric Weeks which feature the original particle tracking routines written by Crocker and Grier (52). The m-file `fit_ellipse.m` was developed by Ohad Gal and is available from the Mathworks website. The file `Localizer.m` is our code which contains numerous functions for executing the analysis.

To run the software, type:

```
output= Localizer('brightfield_prefix', 'fluorescent_prefix', first_file_number,
last_file_number, interactive_logical, ellipse_spacing)
```

The 6 inputs are:

brightfield_prefix: The filename of the brightfield image without the file extension or file number (e.g., for a file named ‘RPAR_bright_1.tif’ the prefix would be ‘RPAR_bright_’).

fluorescent_prefix: The filename of the fluorescent image without the file extension or file number (e.g., for a file named ‘RPAR_TRITC_1.tif’ the prefix would be ‘RPAR_TRITC_’).

first_file_number: The number of the first file that the software is to analyze (e.g., `first_file_number = 1` to start with ‘RPAR_bright_1.tif’ and ‘RPAR_TRITC_1.tif’).

last_file_number: The number of the last file that the software should analyze. (e.g., `last_file_number = 10` to end with ‘RPAR_bright_10.tif’ and ‘RPAR_TRITC_10.tif’).

⁴⁰To do this, imaging system specifications must be known (e.g., camera resolution, objective NA and emission wavelength of each fluorescent channel).

⁴¹We have developed an ImageJ script that automatically opens each image and the appropriate PSF file, performs deconvolution, and then saves the output. Our automated deconvolution script for ImageJ is available on the website. For displaying images we use a secondary processing step that includes the ImageJ commands “Background Subtraction” and “Smooth”. This step removes noise and allows for easy discrimination of fluorescent NPs.

interactive_logical: Set this to 1 if you want the software to write a TIFF file showing the results; set to 0 if you just want the results as a text file.

ellipse_spacing: This parameter sets how thick, in pixels, each cell region (distance between colored lines in Fig. 5B, C) should be. We recommend using a pixel value that corresponds to 2.5 μm .

To run the software using the test images from our website:

```
output= Localizer('RPAR_bright_', 'RPAR_TRITC_', 1, 2, 1, 10)
```

When the program is run it will take the user through 5 steps:

1. Clicking 2 opposing corners of an empty region of the image for determining the background fluorescence value (this number will be used to normalize the fluorescent results of each image).
2. Identifying the number of cells in a given image and cropping each of them by clicking on two opposing corners.
3. Identifying the boundary of a cell by clicking on points on each side of the cell and hitting enter after clicking a side.
4. Identifying the nuclear membrane by clicking around it.
5. Setting the parameters for identifying particles which include the intensity threshold for identifying a particle and the minimum distance between particles. These parameters are direct inputs for Eric Week's `pkfnd.m` and `cntrd.m`. The structure `output` contains the following 8 arrays, where each array element is a data point for a region of the cell:

output.average_NPs_region: The average number of NPs per region.

output.ERROR_NPs: The statistical error of the average number of NPs per region.

output.averge_F_region: The total fluorescence intensity of each region (averaged over the number of cells analyzed).

output.ERROR_F_in_region: The statistical error for the average fluorescence intensity each region.

Output.average_NP_perpix_region: The average number of NPs per region normalized by the average number of pixels per region.

output.ERROR_NP_perpix_region: The statistical error of NPs per region normalized by the average number of pixels per region.

output.average_F_perpix_region: The average fluorescence intensity value per pixel in each region.

output.ERROR_F_perpix_region: The statistical error of the average fluorescence intensity per pixel in each region.

The user has the choice of accessing the results in the Matlab command window by calling the output structure and desired array (e.g., type “*output.average_NPs_region*”) or using the text file that the program will write upon completion. The text file is titled using “*fluorescent_prefix*”. For example, the data above would result in a text file called *RPAR_TRITC_DATA.txt* being created.

3.4.3. Measuring NP-endosomal marker colocalization—Colocalization analysis contains similar features to the localization pipeline but the raw data for the GFP channel can be used to automatically define cell boundaries. Furthermore, subtracting the NP image from the GFP image can generate an image whose boundary defines the intracellular environment, allowing the program to easily disregard any NPs which are not internalized. Our merged fluorescent micrographs contain the lipid signal in the first channel, the Rab signal in the second channel and the DNA signal in the third channel. We define objects as liposomes if they show fluorescence in the first channel but not the third. NPs are defined as objects which fluoresce in the first and third channel.

1. Generate relevant images for analysis using image processing. Image 1: A 3D stack of merged fluorescent images where the second channel is a marker for the organelle (e.g., Rab-GFP or LysoTracker) and the first and third channels are nanoparticle labels (*see* Fig. 6A for an example). Image 2: A 3D stack of the GFP channel that has had its contrast adjusted so that it is nearly a threshold binary image. Image 2 will be used to locate the boundary of the cell. The 2 sets of images should have the following naming convention:
 1. Image 1: FirstHalf_1_merged.tif, FirstHalf_2_merged.tif, ...
 2. Image 2: FirstHalf_1_GFP.tif, FirstHalf_2_GFP.tif, ...
2. Run the program by typing `output=Colocalize('First_Half_FileName', 'Second_Half_Merged_Filename', 'Second_Half_GFP_Filename', num_files, coloc_threshold)`. The 5 input parameters are:

First_Half_FileName: The first half of all filename; everything that comes before the file number.

Second_Half_Merged_Filename: The second half of the merged images' filenames; everything that comes after the file number.

Second_Half_GFP_Filename: The second half of the GFP images' filenames; everything that comes after the file number.

num_files: The number of images that will be analyzed.

coloc_threshold: The minimum distance between a nanoparticle and endosome for it to be considered colocalized

(in pixels). We suggest using a pixel length that corresponds to a length of 500 nm.

3. Identify the number of cells in an image and crop individual cells in the image by clicking opposing corners of a region of interest.
4. Input the slice numbers that correspond to the bottom and top of the volume of interest.
5. Mask relevant regions of the image by around the region you would like to mask (forming a polygon) and then double clicking in the center of the user-defined polygon.
6. Input relevant parameters for detecting cell boundary and confirm for parameters for each slice of the stack. The program will prompt the user for 2 parameters *Threshold* and *Minsize*. *Threshold* refers to the minimum intensity value of a pixel that should be considered inside the cell. *Minsize* refers to the smallest fluorescent object that should be considered inside a cell. *Minsize* is useful for images that contain extracellular fluorescent debris. One novel feature of the software is that it will subtract the image of the particles from the thresholded GFP image that is used to detect the cell boundary. By doing this, particles which are bound to the surface are excluded from the colocalization analysis.
7. Set threshold and minimum inter-particle distance for locating particles. Each channel can have its own particle location parameters defined.
8. The results are written to a text file that contains:
 1. The average number and standard deviation of liposomes per cell.
 2. The average number and standard deviation of liposomes colocalized with an endosomal marker per cell.
 3. The average number and standard deviation of CL–DNA NPs per cell.
 4. The average number and standard deviation of CL–DNA NPs colocalized with an endosomal marker per cell.
 5. The text file also contains the results for each cell analyzed. A 2D TIFF showing the locations of all four signals is also written for each cell.

Acknowledgments

This work was supported by the National Institutes of Health (NIH) under grant number R01 GM59288 (transfection efficiency and co-localization studies with Rab GTPases) and the National Science Foundation (NSF) under grant number DMR-1401784 (nanoparticle imaging and automated image analysis). The Rab5-Q79L-GFP pDNA was a gift from the Weimbs laboratory at UC-Santa Barbara.

References

1. Seeton, JM.; Templer, RM. Polymorphism of Lipid-Water Systems. In: Lipowsky, R.; Sackmann, E., editors. Handbook of Biological Physics. Vol. 1. Wiley; New York: 1995.
2. Feigenson GW. Phase behavior of lipid mixtures. *Nat Chem Bio.* 2006; 2:560–563. [PubMed: 17051225]
3. van Meer G, Voelker DR, Feigenson GW. Membrane lipids: where they are and how they behave. *Nat Rev Mol Cell Biol.* 2008; 9:112–114. [PubMed: 18216768]
4. Bangham AD, Horne RW. Negative staining of phospholipids and their structural modification by surface-active agents as observed in the electron microscope. *J Mol Biol.* 1964; 8:660–668. [PubMed: 14187392]
5. Gregoriadis G, Leathwood PD, Ryman BE. Enzyme entrapment in liposomes. *FEBS Lett.* 1971; 14:95–99. [PubMed: 11945728]
6. Greogriadis G, Ryman BB. Fate of protein-containing liposomes injected into rats – approach to treatment of storage diseases. *Eur J Biochem.* 1972; 23:485–491.
7. Gregoriadis G. Carrier potential of liposomes in biology and medicine. *New Engl J Med.* 1976; 295:704–765. [PubMed: 958245]
8. Pagano RE, Weinstein JN. Interactions of liposomes with mammalian cells. *Ann Rev Biophys Bioeng.* 1978; 7:435–568. [PubMed: 352245]
9. Felgner PL, Gader TR, Holm M, Roman R, Chan HW, Wenz M, Northrop JP, Ringold GM, Danielsen M. Lipofection: A highly efficient, lipid-mediated DNA transfection procedure. *Proc Nat Acad Sci USA.* 1987; 90:11307–11311.
10. Lasic, DD. Liposomes in Gene Delivery. CRC Press; Boca Raton: 1994.
11. Lasic, DD.; Martin, FJ., editors. Stealth liposomes. CRC Press; Boca Raton: 1995.
12. Klibanov AL, Maruyama K, Torchilin VP, Huang L. Amphiphatic polyethyleneglycols effectively prolong the circulation of liposomes. *FEBS Lett.* 1990; 268:235–237. [PubMed: 2384160]
13. Blume G, Cevc G. Liposomes for the sustained drug release in vivo. *Biochim Biophys Acta – Biomembranes.* 1990; 1029:91–97.
14. Abuchowski A, van Es T, Palczuk C, Davis FF. Alteration of Immunological Properties of Bovine Serum Albumin by Covalent Attachment of Polyethylene Glycol. *J Biol Chem.* 1977; 252:1578–3581.
15. Du H, Chandaroy P, Hui SW. Grafted poly-(ethylene glycol) on lipid surfaces inhibits protein adsorption and cell adhesion. *Biochim Biophys Acta – Biomembranes.* 1997; 1326:236–248.
16. Kuhl TL, Leckband DE, Lasic DD, Israelachvili JN. Modulation of interaction forces between bilayers exposing short-chained ethylene oxide headgroups. *Biophys J.* 1994; 66:1479–1488. [PubMed: 8061197]
17. Kenworthy AK, Hristov K, Needham D, McIntosh TH. Range and magnitude of the steric pressure between bilayers containing phospholipids with covalently attached poly(ethylene glycol). *Biophys J.* 1995; 68:1921–1936. [PubMed: 7612834]
18. Lasic, DD. Liposomes: from Physics to Applications. Elsevier; San Diego: 1993.
19. Safinya CR, Ewert KK, Majzoub RN, Leal C. Cationic liposome-nucleic acid complexes for gene delivery and gene silencing. *New J Chem.* 2014; 38:5164–5172.
20. Noble GT, Stefanick JF, Ashley JD, Kiziltepe T, Bilgicer B. Ligand-targeted liposome design: challenges and fundamental considerations. *Trends in Biotechnol.* 2014; 32:32–45.
21. Pearce TR, Shroff K, Kokkoli E. Peptide Targeted Lipid Nanoparticles for Anticancer Drug Delivery. *Adv Mat.* 2012; 24:3803–3822.
22. Radler JO, Koltover I, Salditt T, Safinya CR. Structure of DNA-cationic liposome complexes: DNA intercalation in multilamellar membranes in distinct interhelical packing regimes. *Science.* 1997; 275:810–814. [PubMed: 9012343]
23. Koltover I, Salditt T, Radler JO, Safinya CR. An inverted hexagonal phase of cationic liposome-DNA complexes related to DNA release and delivery. *Science.* 1998; 281:78–81. [PubMed: 9651248]

24. Koltover I, Salditt T, Safinya CR. Phase diagram, stability and overcharging of lamellar cationic lipid-DNA self-assembled complexes. *Biophys J*. 1999; 77:915–924. [PubMed: 10423436]
25. Martin-Herranz A, Ahmad A, Evans HM, Ewert KK, Schulze U, Safinya CR. Surface functionalized cationic lipid-DNA complexes for gene delivery: PEGylated lamellar complexes exhibit distinct DNA-DNA interaction regimes. *Biophys J*. 2004; 96:1160–1168. [PubMed: 14747350]
26. Ewert KK, Evans HM, Zidovska A, Boussein NF, Ahmad A, Safinya CR. A columnar phase of dendritic lipid-based cationic liposome-DNA complexes for gene delivery: Hexagonally ordered cylindrical micelles embedded in a DNA honeycomb lattice. *J Am Chem Soc*. 2006; 128:3998–4006. [PubMed: 16551108]
27. Shirazi RS, Ewert KK, Leal C, Majzoub RN, Boussein NF, Safinya CR. Synthesis and characterization of degradable multivalent cationic lipids with disulfide-bond spacers for gene delivery. *Biochim Biophys Acta – Biomembranes*. 2011; 1808:2156–2166.
28. Silva BFB, Majzoub RN, Chan CL, Li Y, Olsson U, Safinya CR. PEGylated cationic liposome-DNA complexation in brine is pathway dependent. *Biochim Biophys Acta – Biomembranes*. 2014; 1838:398–412.
29. Helfrich W. Elastic properties of lipid bilayers – Theory and Possible Experiments. *Zeitschrift Nature*. 1973; C28:693–703.
30. Seddon JM. Structure of the Inverted Hexagonal Phase and non-Lamellar Phase Transitions of Lipids. *Biochim Biophys Acta*. 1989; 1031:1–69. [PubMed: 2407291]
31. Gruner SM. Stability of Lyotropic Phases with Curved Interfaces. *J Phys Chem*. 1989; 93:7562–7570.
32. Israelachvili, JN. *Intermolecular and Surface Forces*. 2. Academic Press; London: 1992.
33. Safinya CR, Sirota EB, Roux D, Smith GS. Universality in Interacting Membranes: The Effect of Cosurfactants on the Interfacial Rigidity. *Phys Rev Lett*. 1989; 62:1134–1137. [PubMed: 10039585]
34. Boussein NF, McAllister CS, Ewert KK, Samuel CE, Safinya CR. Structure and gene silencing activities of monovalent and pentavalent cationic lipid vectors complexed with siRNA. *Biochemistry*. 2007; 46:4786–4792.
35. Leal C, Boussein NF, Ewert KK, Safinya CR. Highly efficient gene silencing activity of siRNA embedded in a nanostructured gyroid cubic lipid matrix. *J Am Chem Soc*. 2010; 132:16841–16847. [PubMed: 21028803]
36. Leal C, Ewert KK, Shirazi RS, Boussein NF, Safinya CR. Nanogyroids Incorporating Multivalent Lipids: Enhanced Membrane Charge Density and Pore Forming Ability for Gene Silencing. *Langmuir*. 2011; 27:7691–7697. [PubMed: 21612245]
37. Majzoub RN, Chan CL, Ewert KK, Silva BFB, Liang KS, Jacovetty EL, Carragher B, Potter CS, Safinya CR. Uptake and transfection efficiency of PEGylated cationic liposome-DNA complexes with and without RGD-tagging. *Biomaterials*. 2014; 35:4996–5005. [PubMed: 24661552]
38. Majzoub RN, Ewert KK, Jacovetty EL, Carragher B, Potter CS, Li Y, Safinya CR. Patterned Threadlike Micelles and DNA-Tethered Nanoparticles: A Structural Study of PEGylated Cationic Liposome–DNA Assemblies. *Langmuir*. 2015; 31:7073–7079. [PubMed: 26048043]
39. Lin AJ, Slack NL, Ahmad A, George CX, Samuel CE, Safinya CR. Three-dimensional imaging of lipid gene carriers: Membrane charge density controls universal transfection behavior in lamellar cationic liposome-DNA complexes. *Biophys J*. 2003; 83:3307–3316. [PubMed: 12719260]
40. Ahmad A, Evans HM, Ewert KK, George CX, Samuel CE, Safinya CR. New multivalent cationic lipids reveal bell curve for transfection efficiency versus membrane charge density: lipid–DNA complexes for gene delivery. *J Gene Med*. 2005; 7:739–748. [PubMed: 15685706]
41. Ruoslahti E, Bhatia SN, Sailor MJ. Targeting of drugs and nanoparticles to tumors. *J Cell Bio*. 2010; 188:759–768. [PubMed: 20231381]
42. Ruoslahti E. RGD and other recognition sequences for integrins. *Annu Rev Cell Dev Bio*. 1996; 12:697–715. [PubMed: 8970741]
43. Temming K, Schiffelers RM, Molema G, Kok RJ. RGD-based strategies for selective delivery of therapeutics and imaging agents to the tumor vasculature. *Drug Resist Update*. 2005; 8:381–402.

44. Chan CL, Majzoub RN, Shirazi RS, Ewert KK, Chen YJ, Liang KS, Safinya CR. Endosomal escape and transfection efficiency of PEGylated Cationic Liposome-DNA Complexes Prepared with and Acid-Labile PEG-Lipid. *Biomaterials*. 2012; 33:4928–4935. [PubMed: 22469293]
45. Rehman Z, Hoekstra D, Zuhorn IS. Mechanism of polyplex- and lipoplex-mediated delivery of nucleic acids: real-time visualization of transient membrane destabilization without endosomal lysis. *ACS Nano*. 2013; 7:3767–3777. [PubMed: 23597090]
46. Suh J, Wirtz D, Hanes J. Efficient active transport of gene nanocarriers to the cell nucleus. *Proc Natl Acad Sci USA*. 2003; 100:3878–3882. [PubMed: 12644705]
47. Hama S, Akita H, Ito R, Mizuguchi H, Hayakawa T, Harashima H. Quantitative comparison of intracellular trafficking and nuclear transcription between adenoviral and lipoplex systems. *Mol Ther*. 2006; 13:786–794. [PubMed: 16364692]
48. Akita H, Ito R, Khalil IA, Futaki S, Harashima H. Quantitative Three-Dimensional Analysis of the Intracellular Trafficking of Plasmid DNA Transfected by a Nonviral Gene Delivery System Using Confocal Laser Scanning Microscopy. *Mol Ther*. 2004; 9:443–451. [PubMed: 15006612]
49. Gilleron J, Querbes W, Zeigerer A, Borodvsky A, Marisco G, Schubert U, Manygoats K, Seifert S, Andree C, Stoter M, Epstein-Barash H, Zhang L, Koeliansky V, Fitzgerald K, Fava E, Bickle M, Kalaidzidis Y, Akinc A, Maier M, Zerial M. Image-based analysis of lipid nanoparticle-mediated siRNA delivery, intracellular trafficking and endosomal escape. *Nat Biotech*. 2013; 31:638–646.
50. Sahay G, Querbes W, Alabi C, Eltoukhy A, Sarkar S, Zurenko C, Karagiannis E, Love K, Chen D, Zoncu R, Buganim Y, Schroeder A, Langer R, Anderson D. Efficiency of siRNA delivery by lipid nanoparticles is limited by endocytic recycling. *Nat Biotech*. 2013; 31:653–658.
51. Adil MM, Erdman ZS, Kokkoli E. Transfection Mechanisms of Polyplexes, Lipoplexes, and Stealth Liposomes in $\alpha\beta 1$ Integrin Bearing DLD-1 Colorectal Cancer Cells. *Langmuir*. 2014; 30:3802–3810. [PubMed: 24635537]
52. Crocker JR, Grier DG. Methods of Digital Video Microscopy for Colloidal Studies. *J Colloid Interface Sci*. 1996; 179:298–310.
53. Majzoub RN, Chan CL, Ewert KK, Silva BFB, Liang KS, Safinya CR. Fluorescence microscopy colocalization of lipid-nucleic acid nanoparticles with wildtype and mutant Rab5-GFP: A platform for investigating early endosomal events. *Biochim Biophys Acta – Biomembranes*. 2015; 1848:1308–1318.
54. Rehman Z, Hoekstra D, Zuhorn IS. Protein kinase A inhibition modulates the intracellular routing of gene delivery vehicles in HeLa cells, leading to productive transfection. *J Control Release*. 2011; 156:76–84. [PubMed: 21787817]
55. Sharma VD, Lees J, Hoffman NE, Brailoiu E, Madesh M, Wunder SL, Ilies MA. Modulation of pyridinium cationic lipid-DNA complex properties by pyridinium gemini surfactants and its impact on lipoplex transfection properties. *Mol Pharm*. 2014; 11:545–599. [PubMed: 24377350]
56. Stenmark H. Rab GTPases as coordinators of vesicle traffic. *Nat Rev Mol Cell Bio*. 2009; 10:513–525. [PubMed: 19603039]
57. Costes SV, Daelemans D, Cho EH, Dobbin Z, Pavlakis G, Lockett S. Automatic and Quantitative Measurement of Protein-Protein Colocalization in Live Cells. *Biophys J*. 2004; 86:3993–4003. [PubMed: 15189895]

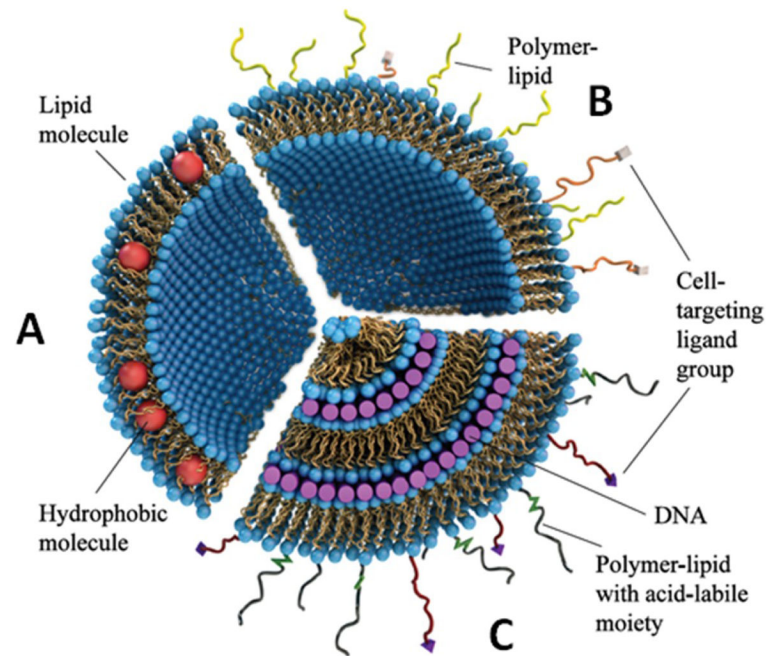


Fig. 1. Evolution of lipid-based drug carriers. (A) Initially liposomes, formed with lipid molecules (shown with blue headgroups and gold tails) were used to trap hydrophobic drugs (red spheres) within the bilayer and hydrophilic drugs in the aqueous interior. (B) Surface-functionalized liposomes typically contain polymer-lipids to inhibit protein binding to the surface. The distal end of the polymer can be chemically-modified with a targeting ligand for organ- and cell-specific targeting. (C) CLs mixed with DNA form condensed CL–DNA complexes with well ordered structure. Polymer lipids can be synthesized with an acid-labile moiety to promote shedding of the polymer at low pH. Reproduced from (19) by permission of The Royal Society of Chemistry (RSC) on behalf of the Centre National de la Recherche Scientifique (CNRS) and the RSC.

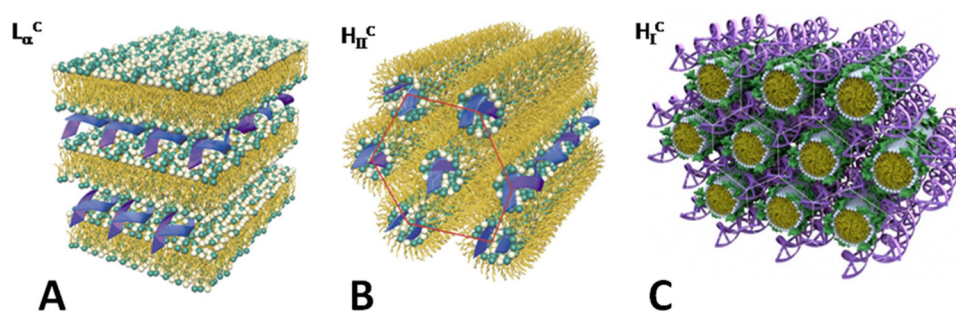


Fig. 2. Internal nanoscale structures of lipid–DNA complexes. **(A)** The lamellar (L_{α}^C) phase forms when the neutral lipid has a cylindrical shape and prefers surfaces with spontaneous curvatures of zero (e.g., DOPC). **(B)** The inverted hexagonal (H_{II}^C) forms when neutral lipids that prefer negative spontaneous curvature such as DOPE are used. **(C)** The hexagonal (H_I^C) phase was discovered upon mixing DOPC and DNA with a custom-synthesized dendritic cationic lipid, MVLBG2 (+16). (A) and (B) reprinted with permission from (23). (C) reprinted with permission from (26). Copyright 2006 American Chemical Society.

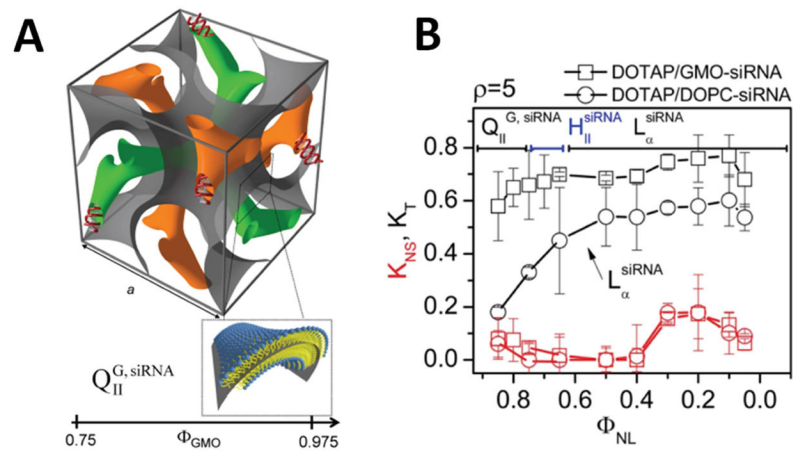


Fig. 3. Double gyroid cubic phase for the delivery of siRNA (A) The unit cell of the cubic phase contains a negative Gaussian surface of lipids (grey) separating 2 water channels that contain siRNA (orange and green). (B) Both lamellar complexes (L_{α}^{siRNA} , circles) and cubic complexes ($Q_{II}^{G, siRNA}$, squares) show low non-specific silencing (red curves) at low membrane charge density but the cubic phase significantly out performs the lamellar phase at total gene knockdown (black curves). Reprinted with permission from (35). Copyright 2010 American Chemical Society.

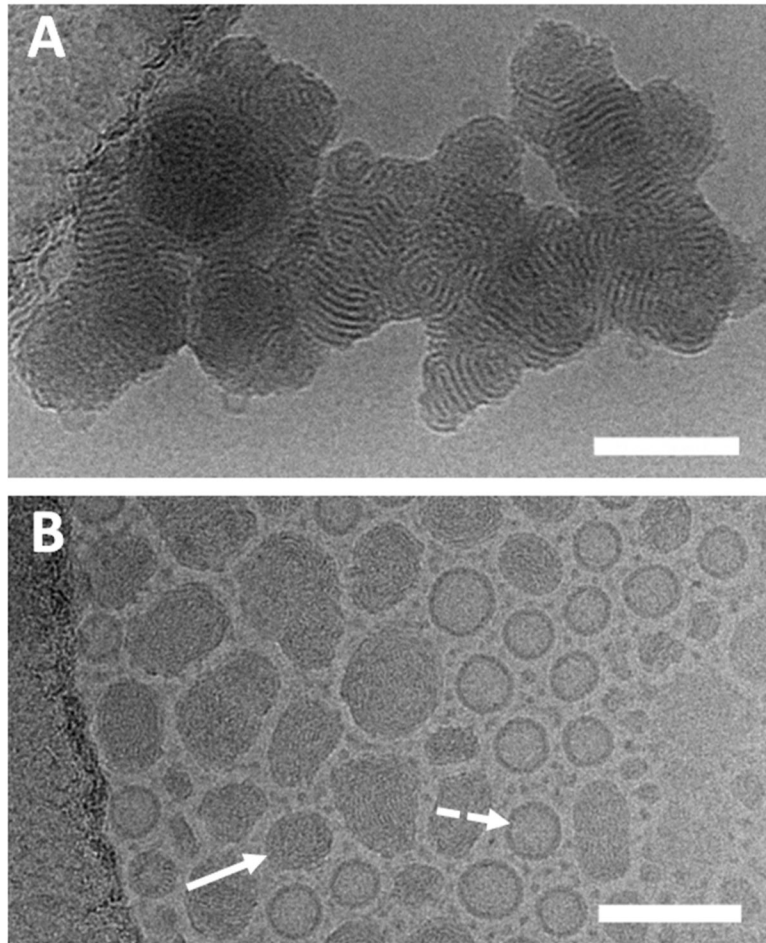


Fig. 4. Cryo-EM micrographs of CL–DNA complexes with and without PEGylation. **(A)** Complexes formed with DOTAP/DOPC at a molar ratio of 80/20 with a charge ratio of 10 in 50 mM NaCl fuse together, forming a large aggregate. **(B)** Stable sub-100 nm NPs form when DNA is mixed with liposomes containing PEG-lipid. Complexes formed with 80/15/5 (molar ratio) DOTAP/DOPC/PEG2K-lipid and charge ratio of 10 in 50 mM NaCl. Electron-dense CL–DNA NPs (solid arrow) coexist with cationic liposomes (dotted arrow). Scale bars correspond to 100 nm. Adapted and reprinted with permission from (37); copyright Elsevier.

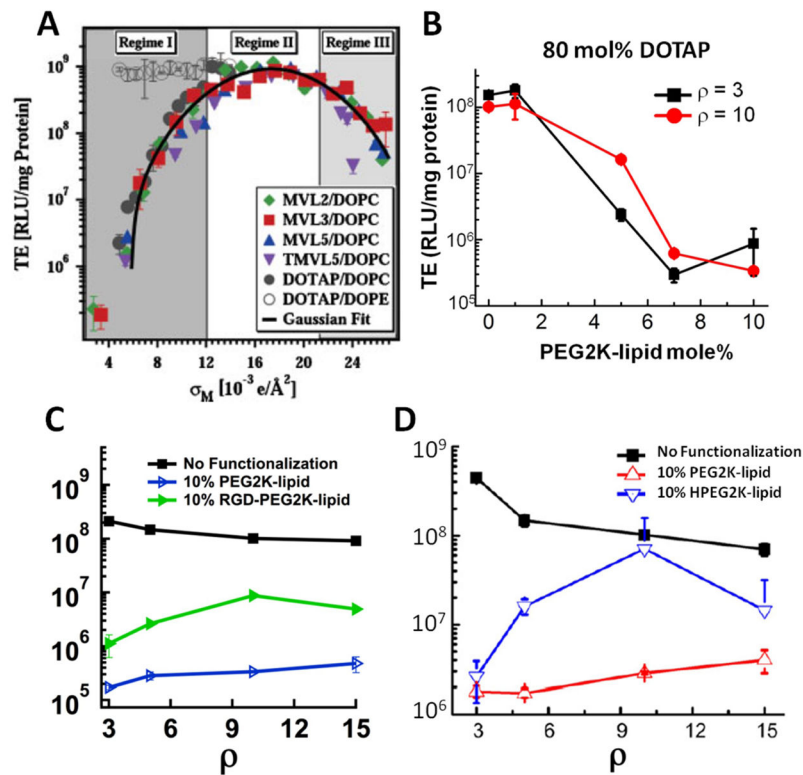


Fig. 5. Transfection Efficiency (TE) of CL-DNA complexes with and without surface functionalization (**A**) The TE of lamellar CL-DNA complexes without functionalization follows a universal curve when plotted against membrane charge density. Filled symbols are different cationic lipids (see legend) and hollow symbols are hexagonal complexes which do not show membrane charge density-dependent TE. (**B**) TE of 80/20-x/x DOTAP/DOPC/PEG2K-lipid complexes where x is noted on the x-axis. (**C**, **D**) The effect of PEGylation, RGD-tagging and HPEG-modification on TE compared to complexes lacking surface modification. (A) is reprinted with permission from (40); copyright 2005 John Wiley & Sons. (B) and (C) are adapted and reprinted with permission from (37); copyright Elsevier. (D) is adapted with permission from (44), copyright Elsevier.

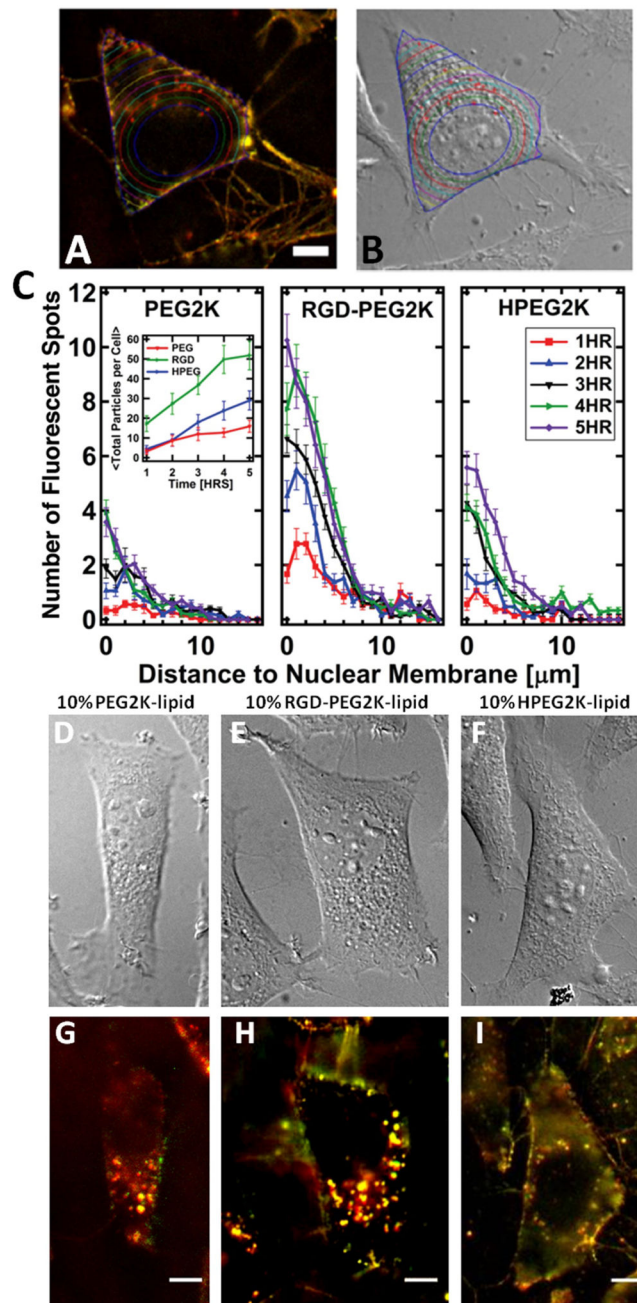


Fig. 6. Measuring intracellular localization and uptake with quantitative fluorescence microscopy. (A, B) A merged fluorescent micrograph (A) and DIC image (B) of a cell that has been incubated with fluorescent NPs. Overlaid on both images are the cell boundary (blue), locations of fluorescent spots (red crosses) and regions defined by distance to the nuclear membrane (various colors). (C) The average number of fluorescent spots at a given distance to the nuclear membrane for CL-DNA NPs containing PEG2K-lipid, RGD-PEG2K-lipid and HPEG2K-lipid. The inset shows total NPs/cell for PEGylated, RGD-tagged and HPEG-modified NPs. (D–I) DIC and fluorescent micrographs of representative live cells used to

generate the data in (C). The surface functionalization is indicated above the micrographs. All scale bars are 10 μm . (A, B, right panel of C) and (left and middle panel of C, D, E, G, H) are adapted and reprinted with permission from (44) and (37), respectively; copyright Elsevier.

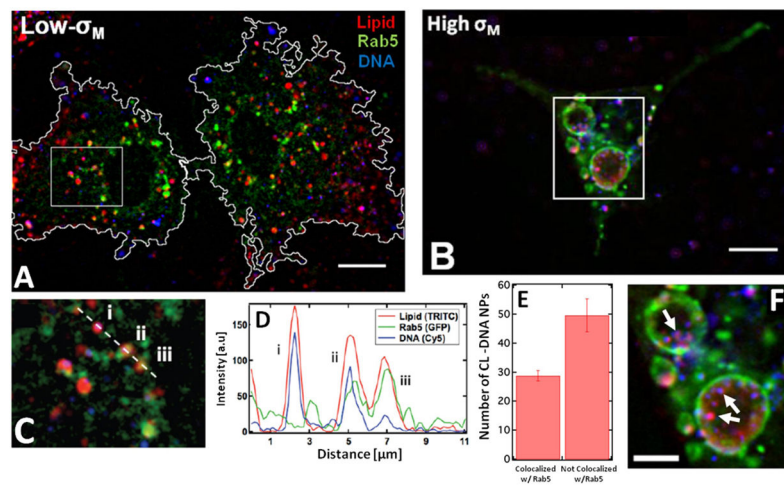


Fig. 7. NPs colocalize with wildtype Rab5-GFP and mutant Rab5-Q79L-GFP (**A, B**) Fluorescent micrographs of L-Cells expressing wildtype (**A**) and mutant (**B**) Rab5-GFP that have been incubated with dual-fluorescently-labeled RGD-tagged NPs for 60 min at 4°C followed by 60 min at 37°C. (**C**) A cropped region from (**A**) showing a NP lacking GFP colocalization (**i**), and 2 NPs colocalized with GFP-Rab5 (**ii, iii**). (**D**) Intensity profile of dashed line in (**C**). (**E**) Average number of NPs colocalized and not colocalized with GFP-Rab5 at 60 min of 37°C incubation (n = 20 cells). (**F**) Cropped region from (**B**) showing giant early endosomes containing individual, resolvable nanoparticles (arrows). Scale bars in (**A, B**) and (**F**) are 10 and 5 μm, respectively. Adapted and reprinted with permission from (53); copyright Elsevier.